Research Article | Vol. 10, No. 7 / 1 July 2020 / Optical Materials Express 1630
Optical Materials EXPRESS

Near-infrared saturable and reverse saturable absorption of ion beam synthesized VO_2 nanocrystals

JAN MUNDRY,[1,*] HUBERT J. KRENNER,[2,3] HELMUT KARL,[4] AND MARKUS BETZ[1]

[1]Experimentelle Physik 2, TU Dortmund University, 44227 Dortmund, Germany
[2]Lehrstuhl für Experimentalphysik I and Augsburg Centre for Innovative Technologies (ACIT), Universität Augsburg, 86159 Augsburg, Germany
[3]Nanosystems Initiative Munich (NIM), 80799 München, Germany
[4]Lehrstuhl für Experimentalphysik IV, Universität Augsburg, 86159 Augsburg, Germany
*jan.mundry@tu-dortmund.de

Abstract: We investigate the nonlinear optical response of a thin film of ion-implanted VO_2 nanocrystals with open aperture z-scans involving femtosecond near-infrared pulses. Beyond the established nonlinearity related to the insulator-metal phase transition of VO_2, the metallic state features a pronounced saturable absorption for 100 fs pulses from a modelocked Yb:fiber source at $\lambda = 1036$ nm. In contrast, we find a pronounced reverse saturable absorption for 90 fs pulses in the telecom window at $\lambda = 1550$ nm. We attribute these nonlinearities to a transient red-shift of the plasmonic resonance of the nanocrystals, in line with the temperature dependence of the linear absorption and the theoretical expectation for electronic heating. Details of the transmissivity characteristics can be tailored by the lattice temperature and/or the size of the nanocrystals. The results hold promise for the use of VO_2 nanocrystals as a saturable absorber, e.g., to mode-locked near-infrared lasers.

1. Introduction

Vanadium dioxide (VO_2) has attracted the interest of researchers for decades since it exhibits an insulator-metal phase transition (IMT) near ambient temperatures (transition temperature of $T_C \approx 68°C$ for bulk crystals). Upon heating, VO_2 undergoes a structural change from a monoclinic to a rutile phase. It is accompanied by a substantial modification of the complex dielectric function and a marked change of the DC electrical conductivity by five orders of magnitude [1]. Closely related, VO_2 nanocrystals (NCs) in their high-temperature phase feature near-infrared plasmonic resonances with properties depending on their size, shape and the host matrix material. VO_2 based structures in general are envisioned for applications such as switchable optical elements [2,3] and the optical control of the phase of light [4]. More recent work incorporates VO_2 into hybrid structures involving, e.g., photonic crystals and waveguides [5,6]. Much less is known about the nonlinear optical properties of VO_2. Z-scan experiments in bulk and nanoscale VO_2 have shown that effective nonlinear optical coefficients extracted for femtosecond pulses at 800 nm are mostly related to an optically induced phase transition rather than to an intrinsic optical nonlinearity of the two individual phases [7].

In this letter, we investigate the near-infrared optical nonlinearity of both the insulating and metallic state of VO_2 NCs of about 100 nm diameter embedded in fused silica. To this end, we perform open aperture z-scans for a wide range of lattice temperatures and two complementary mode-locked fiber laser sources. Such measurements provide direct insight into parameters such as effective saturation intensities and/or effective nonlinear absorption coefficients, i.e., parameters for practical applications such as nonlinear absorbers. The most striking observation

#396099 https://doi.org/10.1364/OME.396099
Journal © 2020 Received 23 Apr 2020; revised 28 May 2020; accepted 28 May 2020; published 17 Jun 2020

Optical Materials EXPRESS

for the metallic state is a pronounced saturable absorption for femtosecond pulses centered at a wavelength of 1036 nm, i.e. in the high-energy flank of the absorptive plasmonic resonance of the NCs. In marked contrast, we find a reverse saturable absorption for femtosecond pulses at a wavelength of 1550 nm, i.e., in the low-energy flank of the plasmonic resonance. Both results are readily understood as arising from a transient red-shift of the plasmonic resonance during the ultrashort light matter interaction window. Such a red-shift upon heating is well known from metallic nanoparticles [8].

2. Sample overview and linear optical properties

The VO_2 NC sample is fabricated by ion beam synthesis by sequential implantation of vanadium (9×10^{16} atoms/cm^2 at 100 keV implantation energy) and oxygen (1.8×10^{17} atoms/cm^2 at 32 keV implantation energy) into a 500 µm thick fused silica substrate [9,10]. Via Raman spectroscopy we can exclude significant amounts of other vanadium oxide phases such as V_2O_5 (data not shown). The formation of roughly spherical NCs with an average diameter of 100 nm and a lateral spacing of about 60 nm happens during a rapid annealing step at a temperature of 1000°C [11]. Specifically, a dense layer of isolated VO_2 nanocrystals (areal density $\sim 10^{10}$ cm^{-2}) is located 85 nm below the surface. These values were estimated from transmission electron micrographs such as the example in Fig. 1(a). As a result, the NCs are well protected from the environment so that they do not suffer from potential detriments like oxidation or hydrophilicity.

Upon heating and/or optical excitation, VO_2 undergoes an abrupt structural change from a monoclinic, insulating state at room temperature to a rutile, metallic phase at elevated temperatures ($T_C \approx 68$°C for bulk crystals) [1,12]. In particular, this IMT is accompanied by a marked change of the complex dielectric function especially in the telecom window [13,14]. In addition, for NCs of high structural quality it exhibits a large hysteresis with a supercooled metallic state persisting almost down to ambient temperatures. These phenomena can be directly seen from the linear optical properties of the sample. Figure 1(b) displays results for the complex refractive index $\boldsymbol{n} = n + ik$ as determined by ellipsometry. In the analysis of the ellipsometry results, the NC layer is modeled as a thin layer of an effective medium with spherical particles embedded into SiO_2 [15]. The dielectric function of VO_2 is included based on an established model with three Lorentz oscillators [16]. The metallic phase features a Mie-type, absorptive resonance as expected for roughly spherical, metallic NCs. It is characterized by an increased imaginary part k and a dispersive signature in the real part n of the complex refractive index. In order to demonstrate the thermal hysteresis, Fig. 1(c) shows the normalized transmissivity for a weak 1036 nm cw-laser beam when the VO_2 NCs are heated and cooled through the phase transition. Upon heating the IMT occurs at ~80°C. The phase transition comes along with a reduction of the transmissivity by as much as ~22%, in line with the ellipsometry data. When the sample is cooled down again, a supercooled metallic state is seen until the transition back to the insulating state happens close to ambient temperatures. The results of electron microscopy (cf. Figure 1(a)) and the temperature range of about 10°C over which the IMT is seen point to a relatively broad distribution of NC sizes. The fairly wide hysteresis is related to the high structural quality of our NCs [17]. In particular, for high quality NCs it is much wider than for VO_2 thin films as, e.g., studied in [18]. Figure 1(d) shows spectrally resolved data for the reduction of the transmissivity in the supercooled metallic state when compared to the insulating state, both at a temperature of 60°C. These results are obtained with a standard setup for (near-infrared) white-light spectroscopy. We note that this setup can also be combined with an oven that permits to record transmissivity spectra at temperatures up to 900°C. The spectrum in Fig. 1(d) is well reproduced by a Gaussian curve with a central photon energy of 0.97 eV and a full with at half maximum of 0.64 eV. We note that the spectral position of this resonance and the characteristics of the hysteresis can be tailored during the fabrication process via e.g. the particle's dimension, shape and the host matrix [11,19–21]. From the theoretical point of view, the position and shape of the plasmonic

Optical Materials EXPRESS

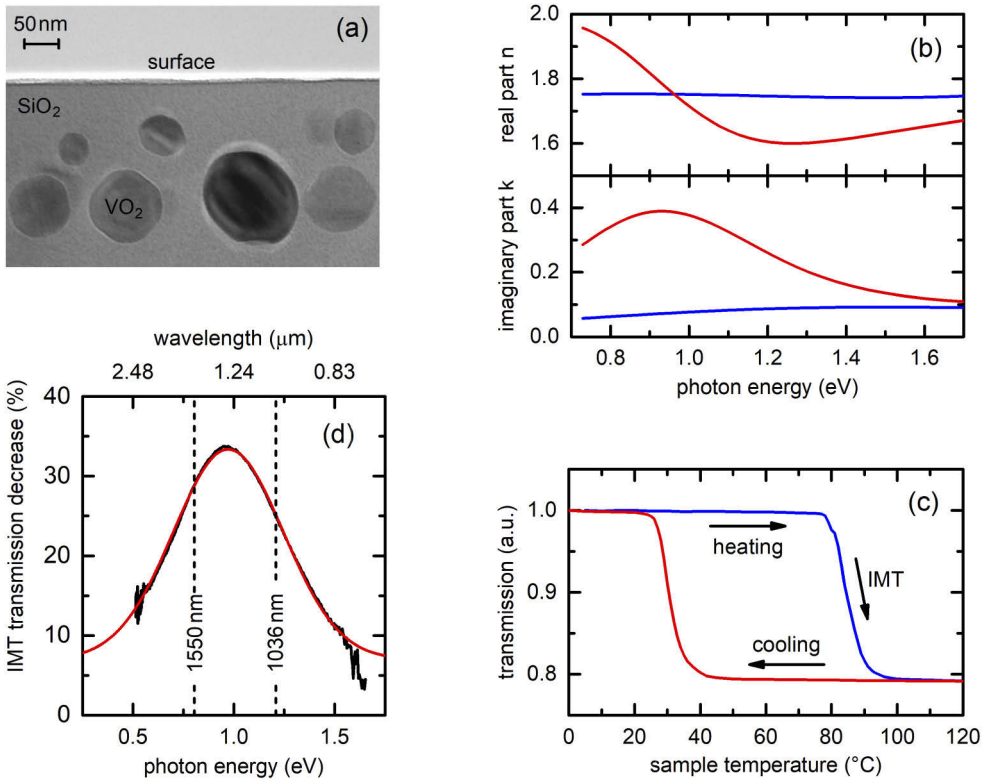

Fig. 1. (a) Cross-section transmission electron microscope image of ion beam synthesized VO_2 nanocrystals (NCs) embedded into a fused silica (SiO_2) matrix. (b) Real and imaginary part of the refractive index of VO_2 NCs in SiO_2 as determined by spectral ellipsometry for different sample temperatures. Blue: 28°C (insulating). Red: 100°C (metallic). (c) Thermally induced insulator-metal phase transition (IMT) and hysteresis recorded by tracking the 1036 nm probe transmission for increasing (blue) and decreasing (red) sample temperatures. The IMT from insulating to metallic VO_2 is triggered at a transition temperature of $T_C \approx 80$°C. Upon cooling, a supercooled metallic phase persists almost down to room temperature. (d) Spectrally resolved data for the relative decrease of the optical transmissivity related to the phase transition from insulating to metallic VO_2 NCs. The red line is a Gaussian fit to the data.

resonance of such NCs can in principle be computed by Maxwell-Garnet theory as described in [21].

Optical Materials EXPRESS

3. Experimental approach

We use the open aperture z-scan technique, pioneered by van Stryland [22] and Sheik-Bahae [23] to determine the nonlinear transmission characteristics of such a layer of VO_2 NCs embedded in fused silica. The measurements are performed at wavelengths of 1036 nm as well as at 1550 nm and at various lattice temperatures corresponding to the different crystallographic phases of VO_2. The first laser source used is a commercial mode-locked Yb:fiber laser (Onefive, Origami HP-10) operating at 4.3 W of average output power. It delivers a train of linearly polarized, transform-limited 100 fs pulses at a repetition rate of 90 MHz and a central wavelength of 1036 nm (central photon energy of 1.20 eV). The second laser source is a commercial mode-locked Er:fiber laser (Toptica, FemtoFiber Scientific) operating at 280 mW of average output power. It delivers a train of linearly polarized, transform-limited 90 fs pulses at a repetition rate of 75 MHz and a central wavelength of 1550 nm (central photon energy of 0.80 eV). Using a half-wave-plate and a polarizing beam splitter cube, a portion of up to a few hundred milliwatts is focused down to a beam waist of 12 µm (9 µm) using a lens with a focal length of 150 mm (75 mm) for the 1036 nm (1550 nm) pulses. These values correspond to the full with at half maximum and are measured with a commercial scanning-slit beam profiler (Thorlabs BP209-IR).

The VO_2 NC sample is located inside a temperature-controlled oven (Covesion OC1 and PV10) that allows for operating temperatures between near-ambient values and 200°C with a high thermal stability. This oven is mounted on a computer-controlled translation stage. Alternatively, the oven can be exchanged by a small vacuum chamber equipped with a Peltier element that allows to cool down the sample to -40°C. All temperatures given throughout the manuscript are related to the SiO_2 substrate. Depending on the irradiance the temperature of the NCs is somewhat higher. We note, however, that the heat conduction into the SiO_2 substrate is much faster than for NCs in a liquid environment where heating, e.g., leads to vapor generation [24,25].

Open aperture z-scans are performed by translating the VO_2 nanocrystal sample through the beam waist of the focused laser beam while measuring the total transmitted intensity [22,23]. Because only the irradiance at the sample is changing upon translation, any (non-destructive) deviation in the total transmitted intensity must be due to saturable absorption or reverse saturable absorption, e.g. related to two-photon absorption. For a more quantitative analysis of selected z-scan traces we employ a phenomenological model based on a nonlinear absorption coefficient and saturation intensity [26,27]. These composite nonlinear absorptions with opposite signs can be phenomenologically combined to a total nonlinear absorption coefficient:

$$\alpha(I) = \frac{\alpha_0}{1 + I/I_S} + \beta I \tag{1}$$

where α_0 is the linear absorption coefficient which is $\alpha_{\text{insulator}}$ = 1.05 x 10^6 m^{-1} and α_{metal} = 3.19 x $10^6 m^{-1}$ at 1036 nm and $\alpha_{\text{insulator}}$ = 5.08 x 10^5 m^{-1} and α_{metal} = 2.78 x 10^6 m^{-1} at 1550 nm, respectively. These values are calculated from the imaginary part k from the complex refractive index, cf. Fig. 1(b). β is the nonlinear absorption coefficient describing multi-photon absorption. I and I_s are the laser intensity and saturation intensity, respectively. In the limit where the nonlinear absorption is restricted to two-photon absorption, associated with the third order nonlinear susceptibility $\chi^{(3)}$, the time-integrated transmitted intensity can be approximated by the following equation [22,23,26–28]:

$$\begin{aligned} T(z) &= \sum_{m=0}^{\infty} \frac{\left[\left(\frac{-\alpha_0}{1+I(z)/I_S} - \beta I(z)\right) L_{eff}\right]^m}{(m+1)^{3/2}} \\ \text{with } I(z) &= \frac{I_0}{1+z^2/z_0^2} \quad \text{and } L_{eff} = \left(1 - e^{-\alpha_0 L}\right) \alpha^{-1} \end{aligned} \tag{2}$$

where β is the two-photon absorption coefficient, L_{eff} is the effective interaction length, z is the longitudinal coordinate with $z = 0$ located at the focal plane, I_0 is the on-axis peak intensity and z_0

Optical Materials EXPRESS

is the Rayleigh length. The sample length L can be estimated by averaging the spherically shaped NCs with an average diameter of 100 nm and a lateral spacing of about 60 nm. We estimate that this configuration corresponds to a homogenous layer of approximately 25 nm thickness.

4. Results and discussion

In the first step we want to give an overview of the rich phenomenology of nonlinear optical processes in VO_2 NCs. Figure 2(a) contains a large number of room temperature z-scan traces recorded for 1036 nm pulses of average powers ranging from 10 mW to 490 mW. The upper power limit is given by the threshold for permanent damage to the NCs occurring at higher power levels. Note that the sample is translated towards more positive z-values.

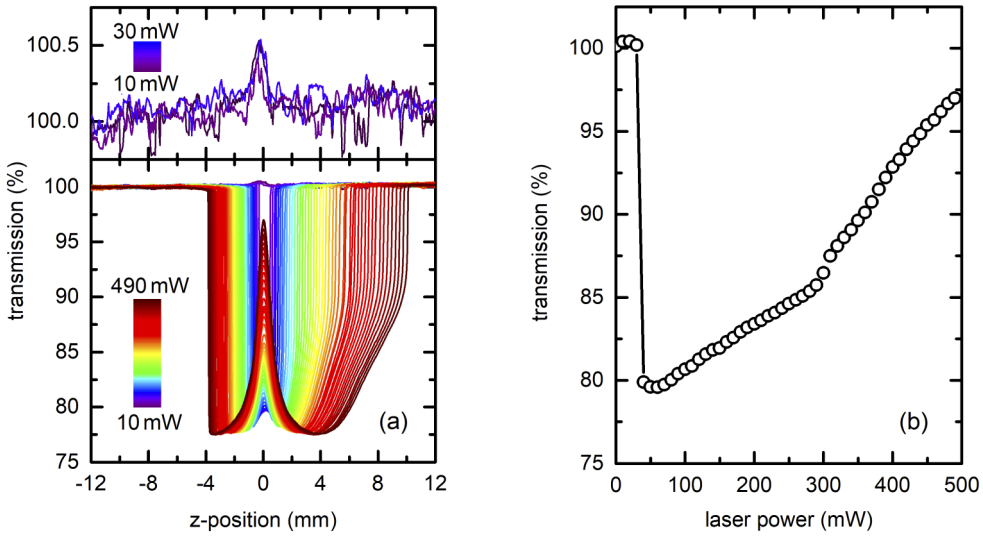

Fig. 2. (a) Series of room temperature z-scan traces recorded for 1036 nm pulses with translation direction to positive z-values. The top panel shows enlarged versions of three low-power z-scans for better visibility. (b) Transmissivity for various powers at the position $z = 0$ extracted from Fig. 2(a). The spectral position of the laser wavelength of this particular measurement with respect to the NCs resonance is shown in Fig. 1(d).

The findings can be grouped into three kinds of optical nonlinearities: (i) For power levels up to 30 mW only a weak positive peak is found around $z = 0$, cf. enlarged z-scan traces in the top panel of Fig. 2(a). It is related to a saturable absorption in the insulating state. (ii) For larger power levels a pronounced dip with minimum transmissivity levels as low as 78% is seen. This behavior is readily explained by a light-induced IMT of VO_2. For somewhat larger powers, the traces become increasingly asymmetric around $z = 0$. This asymmetry arises from the hysteresis of the NCs, i.e. at least a part of the excitation region remains in a supercooled metallic state in the $z > 0$ section. (iii) On top of the IMT-related drop of the transmissivity a marked positive peak is seen which arises from a pronounced saturable absorption of the metallic phase of VO_2. For the largest power levels in Fig. 2(a), the transmissivity at $z = 0$ is even almost restored to the values far away from $z = 0$, i.e., in the low-fluence limit

The main focus of this paper is a careful examination of the nonlinearities (i) and (iii). In contrast, the nonlinearity (ii) is very similar to earlier observations with 800 nm pulses [7] and is not strongly emphasized here. The three different regimes are also evident from Fig. 2(b) where the transmissivities at $z = 0$ are shown. When increasing the power level, a slight increase of the transmissivity is seen, i.e., a saturable absorption occurs. Then, a very sharp IMT-related

Optical Materials EXPRESS

drop of the transmission by ~20% is found. It is followed by an increasing transmission due to the saturable absorption of the metallic phase. Around power levels of 300 mW, a change of the slope is seen in Fig. 2(b). We note that this finding is reproducible. However, we cannot offer an explanation for the change of the nonlinearity to date.

We now compare the above findings to the situation where the sample is translated through the beam waist of the 1550 nm pulse train. Figure 3(a) displays z-scan traces for various power levels ranging from 20 mW to 265 mW. The transmissivity values at $z = 0$ are summarized in Fig. 3(b). For this wavelength the maximum power level is given by the available power of the mode-locked Er:fiber laser. To partially compensate for the lower power levels, we use somewhat tighter focusing as quantified in the description of the experimental setup. The z-scan traces look drastically different from those in Fig. 2. For low power levels, a slight decrease of the transmissivity around $z = 0$ is seen. It arises from a reverse saturable absorption of the insulating state of VO_2. For elevated power levels, the traces are again dominated by the IMT-related sharp drop of the transmissivity. For 1550 nm pulses, the absorption of the metallic phase is slightly stronger when compared to the 1036 nm case. The result is also expected from the data in Fig. 1(d). On top of this nonlinearity, another drop of the transmissivity is observed for power levels > 100 mW. It is related to reverse saturable absorption of the metallic state of VO_2. Remarkably, for the highest available powers the transmission at $z = 0$ drops to values as low as 57% of the value for unfocused pulses.

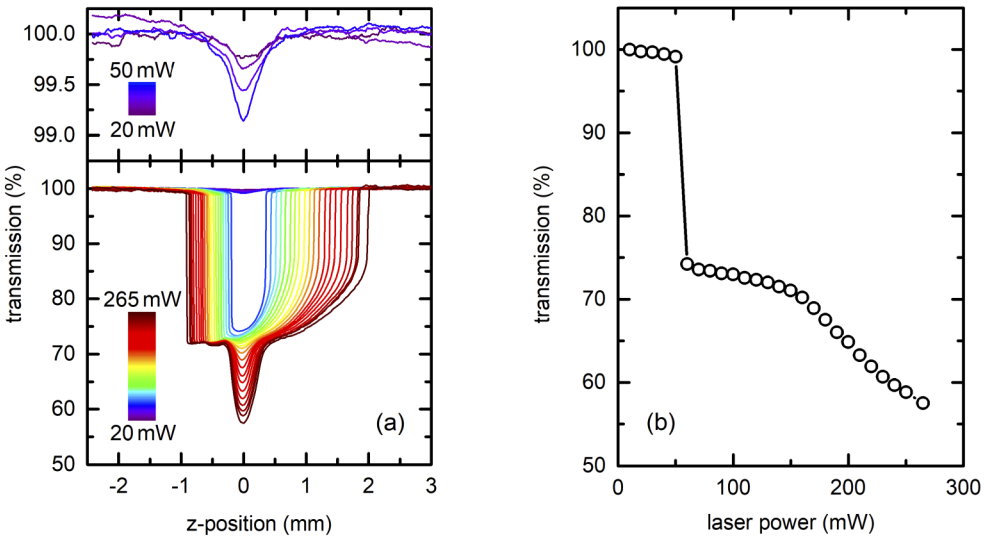

Fig. 3. (a) Series of room temperature z-scan traces recorded for 1550 nm pulses. The sample is translated towards positive z-values. The top panel shows enlarged versions of four low-power z-scans for better visibility. (b) Transmissivity values at $z = 0$ for various power levels, as extracted from Fig. 3(a). The spectral position of the laser wavelength of this particular measurement with respect to the NCs resonance is shown in Fig. 1(d).

The data in Fig. 3(b) show a marked change of their slope at about 160 mW. It is instructive to compare these results to Fig. 2(b). In both cases the change of the slope occurs at a power density of ~2.5 mW/μm^2 and point to a quantitative modification of the optical nonlinearity. Again, this effect is reproducible but still requires further investigation.

The results so far are related to a convolution of the IMT and the optical nonlinearity of both the metallic and insulating state. We now turn towards the central aspect of the paper which is the nonlinearity of the individual states of VO_2 NCs. To investigate the metallic state only, we heat the sample to 100°C, i.e., well above T_C. Figure 4(a) contains z-scan traces for the 1036 nm

Optical Materials EXPRESS

pulse train and the same power range as used for the data in Fig. 2(a). For all power levels, saturable absorption is found. For the highest irradiances the transmittance almost recovers to the value seen for the insulating state (cf. Figure 2(a)). In a complex material such as VO_2 NCs, this saturable absorption is probably not related to a standard third-order nonlinearity. However, it is still instructive to extract, e.g., I_s equivalent values from such traces. The extracted values for I_s according to Eq. (2) for the different power levels are summarized in Fig. 4(b) along with an example for such a fit to the data.

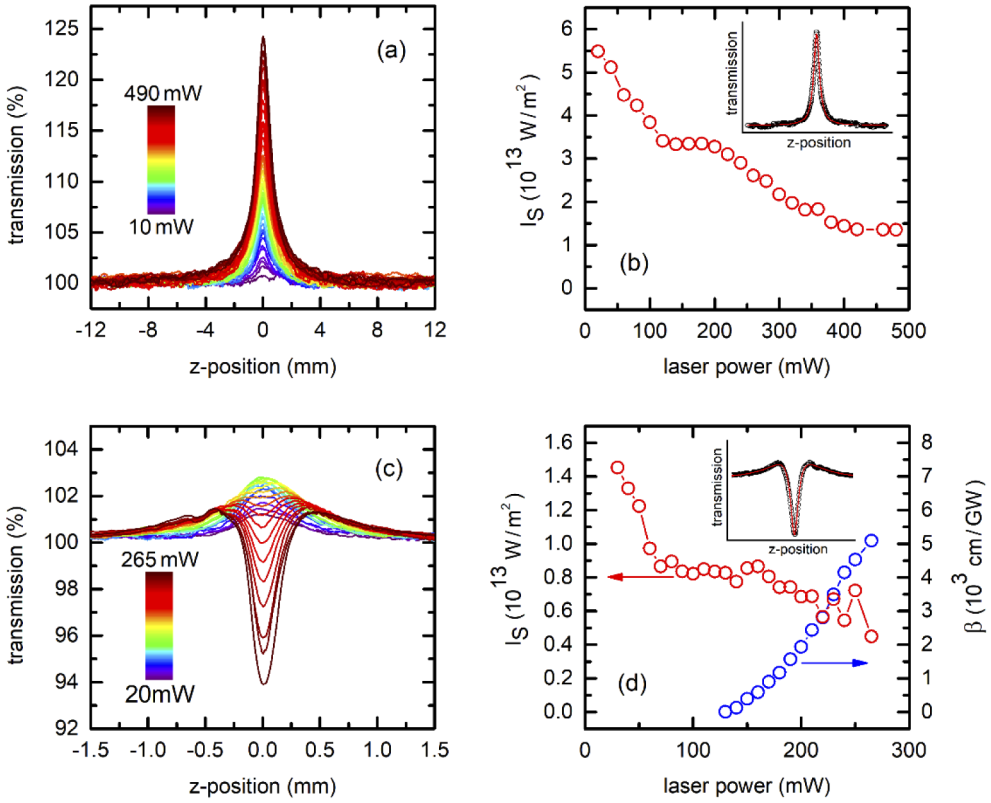

Fig. 4. (a) & (c) Show series of high temperature (T = 100°C > T_C) z-scan traces recorded for (a) 1036 nm and (c) 1550 nm pulses with translation direction to positive z-values. (b) Saturation intensity I_S for VO_2 NCs in the metallic state and 1036 nm laser wavelength extracted from Fig. 4(a) using Eq. (2). (d) Saturation intensity I_S and two-photon absorption coefficient β for VO_2 NCs in the metallic state and 1550 nm laser wavelength extracted from Fig. 4(c) using Eq. (2).

We now compare these results to the optical nonlinearity of the metallic state at 1550 nm. Figure 4(c) contains z-scan traces for the 1550 nm pulse train and the same power range as used for the data in Fig. 3(a). It shows a transition from saturable absorption at low-to-moderate powers to reverse saturable absorption at elevated powers. This saturable absorption is not resolved in the data in Fig. 3(a) as it is probably hidden underneath the large response related to the IMT. The combined saturable and reverse saturable absorption is modeled according to Eq. (2) to yield equivalent I_s and β values. The extracted values for I_s and β for the different power levels are summarized in Fig. 4(d) along with an example for such a fit to the data. In direct comparison to Fig. 4(b), I_s takes values in the same order of magnitude. Also a decrease of I_s for increasing power levels is seen in both cases.

Optical Materials EXPRESS

It is instructive to compare these values for I_s to those of other materials. Our values are comparable or somewhat smaller than the I_s of typical bulk semiconductors [29]. However they are not as small as those of NCs made from noble metals [28,30]. In view of those results, our values for the I_s of VO_2 NCs seem reasonable as those NCs are made from a material of moderate metallic conductivity. Values of β can only be reliably extracted for 1550 nm pulses and power levels beyond 120 mW. They increase with the excitation power and are seen to take values as large as ~5000 cm/GW. As the typical two-photon absorption coefficient of, e.g., prototypical semiconductors such as GaAs, is in the range of 10 cm/GW [31], the observed value for β is unlikely to arise from true two-photon absorption. In metallic systems, however, it is well known that very large values of the apparent two-photon absorption coefficients in z-scan traces can arise from thermal effects [32]. In essence, the front part of the ultrashort laser pulse heats the electronic systems and, thereby, the absorption of the rear part is enhanced. Furthermore the overall power-dependent behavior of β suggests that higher orders of optical nonlinearities contribute to the observed absorption. Therefore Eq. (2) would have to be extended beyond the limit of a bare two-photon process for an accurate description.

At first glance the results presented in the panels 4(a) and 4(c) seem to be contradictory as a metallic system should behave similar irrespective of the exact photon energy in the near-infrared spectral domain. However, the different behavior can be directly related to the plasmonic resonance of the VO_2 NCs and its spectral profile for different temperatures. Figure 5 shows the normalized difference between the metallic phase at different lattice temperatures when compared to the insulating state at room temperature. It shows a clear red-shift and broadening upon heating. This finding is well established, e.g., for gold nanoparticles [8]. In short the red-shift can be largely explained by the thermal expansion of the NCs while the broadening of the resonance is readily explained by enhanced electron-phonon scattering. Certainly the situation of an ultrashort interaction with the NCs is different in the sense that only the electron system is heated while the ~100 fs pulse is present and the timescale is too short for significant thermal expansion. As an example the 1550 nm Er:fiber laser's pulse energy is calculated to be 3.33×10^{-9} J at an average laser power of 250 mW. The illuminated volume of pure VO_2 in the focal plane sums up to be 1.6 μm^3 (c.f. section 3). The rise of the electron temperature can now be estimated from the average kinetic energy taking into account an overall optical absorption of 42% of the laser's pulse energy (c.f. Figure 3(a)). For various values of the electron density in VO_2 found in literature [33–35] the electron temperature ranges from several hundred Kelvin to a few ten thousand Kelvin above ambient temperature. A transient red-shift of the resonance, however, readily explains the different observations in Figs. 4(a) and (c). As shown in the Fig. 5, such a red-shift moves the 1550 nm pulse towards the peak of the absorptive resonance. In contrast, the 1036 nm pulse is shifted away from the resonance explaining the reduced absorption for strong irradiance.

Finally we address the optical nonlinearity of the insulating state. To this end, we cool the sample to -35°C such that (in comparison with the data in Figs. 2 and 3) larger power levels can be used without triggering the IMT. At 1550 nm, power levels of up to 130 mW can be used before the IMT is photo-induced, cf. the dashed graph of Fig. 6(a) that shows the z-scan trace with an optically triggered IMT for a power of 140 mW. For all power levels we find a well-resolved reverse saturable absorption. However it is much weaker than the apparent nonlinearity related to the IMT. Nevertheless the z-scan trace for 130 mW power is indicative of an equivalent two-photon absorption coefficient as large as β = 3510 cm/GW. At 1036 nm, power levels up to 75 mW leave the sample in the insulating state, cf. the dashed graph of Fig. 6(b) that shows the z-scan trace with an optically triggered IMT for a power of 80 mW. The z-scan traces for lower power levels are indicative of rather weak optical nonlinearities with z-scan traces deviating from unity by 1% at most. Surprisingly, the traces exhibit dispersive features which are more likely to occur for closed-aperture z-scans. We have carefully checked that the traces are not related to,

Optical Materials EXPRESS

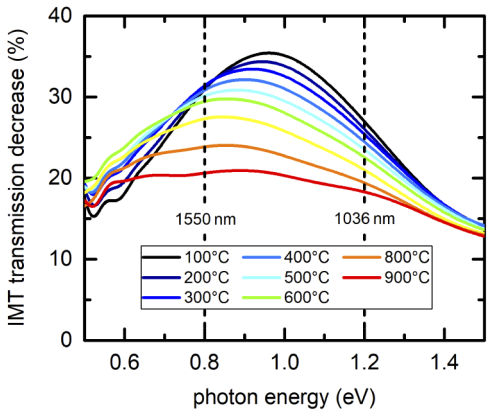

Fig. 5. Evolution of the IMT transmission decrease (normalized transmission difference between the metallic phase and the insulating state) at different lattice temperatures. The visible reduction of the resonance's amplitude partially occurs from a degeneration process of the hot sample in air environment. To partly compensate for this effect, a vertical offset aligns the traces outside the resonance. The sample investigated here originates from a different batch such that center energy, width and amplitude of the resonance slightly differ from the data shown in Fig. 1(d).

e.g., a lensing effect that could arise from the real part of the third-order optical nonlinearity. Instead they are related to some form of photo-induced modification of the NCs that exhibits a hysteretic behavior. Most likely this asymmetric graph originates from a slightly shifted overlap of a saturable absorption (symmetric around $z = 0$) and an optically induced IMT with hysteretic behavior of only a few single nanocrystals ($z > 0$). The latter can be estimated from the positive z-position of the induced phase transition at elevated laser power. In particular, the traces for a z-scan along the negative z-axes leads to traces that are mirrored around $z = 0$. We note that this mirror-symmetry also holds true for z-scan traces where the IMT is photo-induced and the NCs remain in the supercooled metallic state (data not shown). Specifically the IMT leads to asymmetric z-scan traces as shown in Fig. 2(a) or Fig. 3(a).

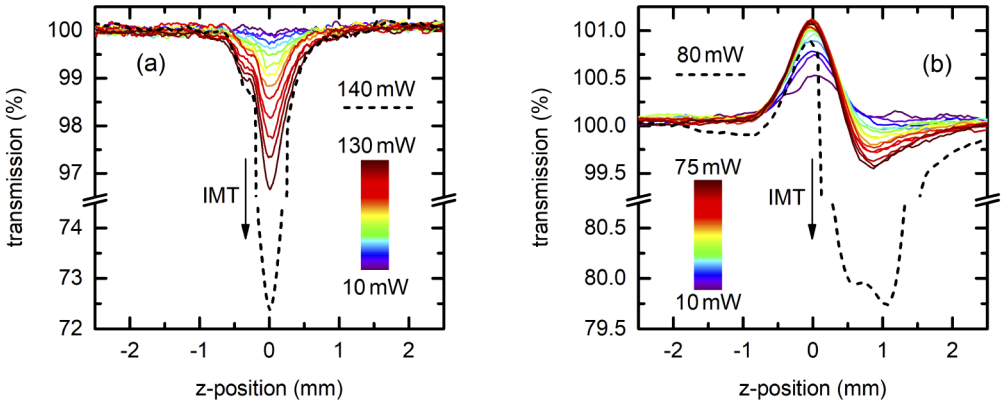

Fig. 6. (a) & (b) Show series of low temperature (T = -35°C < T_C) z-scan traces recorded for (a) 1550 nm and (b) 1036 nm pulses with translation direction to positive z-values. The dashed graphs show z-scan traces with triggered IMT.

Optical Materials EXPRESS

5. Conclusion

In conclusion, the nonlinear optical response of a thin film of ion beam synthesized VO_2 nanocrystals is thoroughly investigated by open aperture z-scan technique involving femtosecond near-infrared pulses. It is found that, beyond the established nonlinearity related to the insulator-metal phase transition of VO_2, the metallic state features a pronounced saturable absorption at $\lambda = 1036$ nm. In marked contrast, a pronounced reverse saturable absorption of the metallic state is found at $\lambda = 1550$ nm. These nonlinearities are attributed to a transient red-shift of the plasmonic resonance of the nanocrystals during the ultrafast light-matter interaction. The insulating state is characterized by a substantial reverse saturable absorption at $\lambda = 1036$ nm and a weak optical nonlinearity at $\lambda = 1550$ nm. A quantitative analysis of the different z-scan traces using a phenomenological model based on nonlinear and/or saturable absorption reveal high equivalent two-photon absorption coefficients of several thousand cm/GW and saturation intensities in the range of 10^{13} W/m^2. These nonlinearities are largely linked to the plasmonic resonances of metallic VO_2 NCs. As this resonance can be custom tailored by, e.g., the NCs' size and host material, our results hold promise to achieve widely adjustable and large optical nonlinearities in the near-infrared, suitable for applications such as saturable absorbers to mode-locked lasers.

Funding

TU Dortmund University Open Access Publishing; Deutsche Forschungsgemeinschaft (TRR 142 (project B02)).

Acknowledgements

The authors acknowledge financial support through the DFG collaborative research center TRR 142 (project B02).

The authors acknowledge financial support by TU Dortmund University within the funding program Open Access Publishing.

Disclosures

The authors declare no conflicts of interest relate to this article.

References

1. F. J. Morin, "Oxides Which Show a Metal-to-Insulator Transition at the Neel Temperature," Phys. Rev. Lett. **3**(1), 34–36 (1959).
2. S. B. Choi, J. S. Kyoung, H. S. Kim, H. R. Park, D. J. Park, B.-J. Kim, Y. H. Ahn, F. Rotermund, H.-T. Kim, K. J. Ahn, and D. S. Kim, "Nanopattern enabled terahertz all-optical switching on vanadium dioxide thin film," Appl. Phys. Lett. **98**(7), 071105 (2011).
3. G. Seo, B.-J. Kim, Y. W. Lee, and H.-T. Kim, "Photo-assisted bistable switching using Mott transition in two-terminal VO_2 device," Appl. Phys. Lett. **100**(1), 011908 (2012).
4. T. V. Son, K. Zongo, C. Ba, G. Beydaghyan, and A. Haché, "Pure optical phase control in vanadium dioxide thin films," Opt. Commun. **320**, 151–155 (2014).
5. A. Rashidi, S. Roshan Entezar, and A. Hatef, "Tunable Multispectral Near-Infrared Absorption with a Phase Transition of VO_2 Nanoparticles Hybridized with 1D Photonic Crystals," Nanotechnology **10**(1088), 1361–6528 (2020).
6. Y. Tan, L. Chen, and D. Wang, "Tunable Picosecond Laser Pulses via the Contrast of Two Reverse Saturable Absorption Phases in a Waveguide Platform," Sci. Rep. **6**(1), 26176 (2016).
7. R. López, R. F. Haglund Jr., and L. C. Feldman, "Optical nonlinearities in VO_2 nanoparticles and thin films," Appl. Phys. Lett. **85**(22), 5191–5193 (2004).
8. O. A. Yeshchenko, I. S. Bondarchuk, V. S. Gurin, I. M. Dimitruk, and A. V. Kotko, "Temperature dependence of the surface plasmon resonance in gold nanoparticles," Surf. Sci. **608**, 275–281 (2013).
9. J. Zimmer, A. Wixforth, H. Karl, and H. J. Krenner, "Ion beam synthesis of nanothermochromic diffraction gratings with giant switching contrast at telecom wavelengths," Appl. Phys. Lett. **100**(23), 231911 (2012).
10. M. Rini, A. Cavalleri, R. W. Schoenlein, R. López, L. C. Feldman, R. F. Haglund Jr., L. A. Boatner, and T. E. Haynes, "Photoinduced phase transition in VO_2 nanocrystals: ultrafast control of surface-plasmon resonance," Opt. Lett. **30**(5), 558–560 (2005).

Optical Materials EXPRESS

11. H. Karl, J. Dreher, and B. Stritzker, "Semiconductor-metal Phase Transition in Doped Ion Beam Synthesized VO_2 Nanoclusters," Mater. Res. Soc. Symp. Proc. **1174**, 1174-V06-35 (2009).
12. A. Zylbersztejn and N. F. Mott, "Metal-insulator transition in vanadium dioxide," Phys. Rev. B **11**(11), 4383–4395 (1975).
13. H. W. Verleur, A. S. Barker Jr., and C. N. Berglund, "Optical properties of VO_2 between 0.25 and 5 eV," Phys. Rev. **172**(3), 788–798 (1968).
14. M. Tazawa, P. Jin, and S. Tanemura, "Optical constants of $V_{1-x}W_xO_2$ films," Appl. Opt. **37**(10), 1858–1861 (1998).
15. D. Stroud, "The effective medium approximations: Some recent developments," Superlattices Microstruct. **23**(3-4), 567–573 (1998).
16. H. Kakiuchida, P. Jin, S. Nakao, and M. Tazawa, "Optical Properties of Vanadium Dioxide Film during Semiconductive-Metallic Phase Transition," Jpn. J. Appl. Phys. **46**(No. 5), L113–L116 (2007).
17. K. Appavoo, D. Y. Lei, Y. Sonnefraud, B. Wang, S. T. Pantelides, S. A. Maier, and R. F. Haglund Jr., "Role of Defects in the Phase Transition of VO_2 Nanoparticles Probed by Plasmon Resonance Spectroscopy," Nano Lett. **12**(2), 780–786 (2012).
18. M. Currie, V. D. Wheeler, B. Downey, N. Nepal, S. B. Qadri, J. A. Wollmershauser, J. Avila, and L. Nyakiti, "Asymmetric hysteresis in vanadium dioxide thin films," Opt. Mater. Express **9**(9), 3717–3728 (2019).
19. R. López, L. Feldman, and R. F. Haglund Jr., "Size-dependent optical properties of VO_2 nanoparticle arrays," Phys. Rev. Lett. **93**(17), 177403 (2004).
20. W. Zeng, N. Chena, and W. Xie, "Research progress on the preparation methods for VO_2 nanoparticles and their application in smart windows," CrystEngComm **22**(5), 851–869 (2020).
21. S.-Y. Li, G. A. Niklasson, and C. G. Granqvist, "Nanothermochromics: Calculations for VO_2 nanoparticles in dielectric hosts show much improved luminous transmittance and solar energy transmittance modulation," J. Appl. Phys. **108**(6), 063525 (2010).
22. E. W. Van Stryland, M. A. Woodall, H. Vanherzeele, and M. J. Soileau, "Energy band-gap dependence of two-photon absorption," Opt. Lett. **10**(10), 490–492 (1985).
23. M. Sheik-Bahae, A. A. Said, T. H. Wei, D. J. Hagan, and E. W. Van Stryland, "Sensitive measurement of optical nonlinearities using a single beam," IEEE J. Quantum Electron. **26**(4), 760–769 (1990).
24. O. Neumann, A. S. Urban, J. Day, S. Lal, P. Nordlander, and N. J. Halas, "Solar Vapor Generation Enabled by Nanoparticles," ACS Nano **7**(1), 42–49 (2013).
25. Z. Fang, Y.-R. Zhen, O. Neumann, A. Polman, F. J. G. de Abajo, P. Nordlander, and N. J. Halas, "Evolution of light-induced vapor generation at a liquid-immersed metallic nanoparticle," Nano Lett. **13**(4), 1736–1742 (2013).
26. X. Zheng, Y. Zhang, R. Chen, X. Cheng, Z. Xu, and T. Jiang, "Z-scan measurement of the nonlinear refractive index of monolayer WS_2," Opt. Express **23**(12), 15616–15623 (2015).
27. J. Wang, B. Gu, H.-T. Wang, and X.-W. Ni, "Z-scan analytical theory for material with saturable absorption and two-photon absorption," Opt. Commun. **283**(18), 3525–3528 (2010).
28. Y. Gao, X. Zhang, Y. Li, H. Liu, Y. Wang, Q. Chang, W. Jiao, and Y. Song, "Saturable absorption and reverse saturable absorption in platinum nanoparticles," Opt. Commun. **251**(4-6), 429–433 (2005).
29. B. Gu, Y.-X. Fan, J. Chen, H.-T. Wang, J. He, and W. Ji, "Z-scan theory of two-photon absorption saturation and experimental evidence," J. Appl. Phys. **102**(8), 083101 (2007).
30. M. Hari, S. Mathew, B. Nithyaja, S. A. Joseph, V. P. N. Nampoori, and P. Radhakrishnan, "Saturable and reverse saturable absorption in aqueous silver nanoparticles at off-resonant wavelength," Opt. Quantum Electron. **43**(1-5), 49–58 (2012).
31. D. A. Kleinman, R. C. Miller, and W. A. Nordland, "Two-photon absorption of Nd laser radiation in GaAs," Appl. Phys. Lett. **23**(5), 243–244 (1973).
32. N. Rotenberg, A. D. Bristow, M. Pfeiffer, M. Betz, and H. M. van Driel, "Nonlinear absorption in Au films: Role of thermal effects," Phys. Rev. B **75**(15), 155426 (2007).
33. A. S. Barker Jr., H. W. Verleur, and H. J. Guggenheim, "Infrared Optical Properties of Vanadium Dioxide Above and Below the Transition Temperature," Phys. Rev. Lett. **17**(26), 1286–1289 (1966).
34. D. H. Hensler, "Transport Properties of Sputtered Vanadium Dioxide Thin Films," J. Appl. Phys. **39**(5), 2354–2360 (1968).
35. D. Ruzmetov, D. Heiman, B. B. Claflin, V. Narayanamurti, and S. Ramanathan, "Hall carrier density and magnetoresistance measurements in thin film vanadium dioxide across the metal-insulator transition," Phys. Rev. B **79**(15), 153107 (2009).